Journal of Materials Chemistry C

PAPER

Check for updates

A co-solvent exfoliation strategy of quasi-1D electronic grade Ta$_2$Pt$_3$Se$_8$ for enhanced yields in non-toxic low boiling point solvents†

Kyung Hwan Choi,‡[b] Dahoon Kim,‡[a] Jinsu Kang,[a] Chaeheon Woo,[a] Xiaojie Zhang,[a] Yeong Hyeop Kim,[a] Yeongjin Kim,[a] Hyeon-Seok Bang,[ad] Kyung In Kim,[a] Jeong Su Park,[a] Seyoung Jang,[a] Jongwha Chang,[f] Hyung-Suk Oh, [ID][ade] Jae-Hyun Lee, [ID][c] Hak Ki Yu [ID]*[c] and Jae-Young Choi [ID]*[abe]

Ta$_2$Pt$_3$Se$_8$, a quasi-1D van der Waals material, exhibits promising structural and electrical properties, making it a potential candidate for electronic applications. However, the traditional liquid phase exfoliation (LPE) of Ta$_2$Pt$_3$Se$_8$ requires toxic and high boiling point solvents like NMP and DMF, which limits its broader application. In this study, we introduce a co-solvent strategy using an IPA/water mixture to optimize the LPE of Ta$_2$Pt$_3$Se$_8$. By adjusting the volume ratios, the total surface tension, polar-to-dispersive (P/D) ratio and dielectric constant of the co-solvent were fine-tuned, achieving high exfoliation efficiency. Field-effect transistors (FETs) were successfully fabricated and exhibited a field-effect mobility of 6.76 cm^2 V^{-1} s^{-1} and I_{on}/I_{off} greater than 10^3. The results demonstrate that this co-solvent approach provides a lower-toxicity alternative for LPE while maintaining high exfoliation yields.

Introduction

Solution-based processing of low-dimensional materials has attracted significant interest for decades as a powerful route for scalable, large-scale production across a wide variety of applications.[1–4] This method is mainly divided into bottom-up and top-down approaches. In the bottom-up approach, materials are synthesized by building up from atoms or molecules into larger structures/assemblies in the presence of liquid-phase precursors.[5] Representative synthesis methods include hydrothermal/solvothermal reactions, self-assembly, sol–gel, and colloidal synthesis, which can be applied to various materials ranging from zero-dimensional (*e.g.*, AuNPs,[6] CdTe[7]) to

one-dimensional (1D) (*e.g.*, ZnO,[8] tellurium,[9,10] Nb$_2$Se$_9$[11]) and two-dimensional (2D) (*e.g.*, MXenes,[12,13] MoS$_2$[14]) structures.[15] On the other hand, the top-down approach involves breaking down the initial 3D crystal structures into smaller units in liquid media. This method is cost-effective and straightforward, making it the most widely used approach in research on 1D and 2D van der Waals (vdW) materials.[1,16] Particularly, 2D transition metal dichalcogenides (TMDCs) have been actively studied in this top-down solution processing due to their intriguing electronic and optoelectronic properties.[17–19] Additionally, 1D vdW materials have gained significant attention, and extensive research has been conducted on the top-down solution processing to expand their range of applications.[20–22]

Ta$_2$Pt$_3$Se$_8$ is a quasi-1D vdW material with unique structural and electrical properties, allowing it to be a highly suitable building block for electronic applications. Ta$_2$Pt$_3$Se$_8$ has been utilized for field-effect transistors (FETs) and photodetectors as a promising p-type semiconductor due to its excellent carrier transport and optoelectronic properties.[23–25] In addition, owing to the vdW nature, Ta$_2$Pt$_3$Se$_8$ can be effectively downsized through mechanical exfoliation or liquid phase exfoliation (LPE) depending on the intended applications. Mechanical exfoliation is effective for fundamental studies or when precise alignment is required, but for forming specific structures over large areas or achieving high-yield, large-scale production, LPE is more suitable.[2,26] However, in the case of LPE of Ta$_2$Pt$_3$Se$_8$, a drawback is that it requires solvents like

[a] School of Advanced Materials Science and Engineering, Sungkyunkwan University, Suwon 16419, Korea. E-mail: jy.choi@skku.edu

[b] SKKU Advanced Institute of Nanotechnology (SAINT), Sungkyunkwan University, Suwon 16419, Republic of Korea

[c] Department of Materials Science and Engineering & Department of Energy Systems Research, Ajou University, Suwon 16499, Republic of Korea. E-mail: hakkiyu@ajou.ac.kr

[d] Clean Energy Research Center, Korea Institute of Science and Technology (KIST), Seoul 02792, Republic of Korea

[e] KIST-SKKU Carbon-Neutral Research Center, Sungkyunkwan University, Suwon 16419, Republic of Korea

[f] Department of Internal Medicine, Wayne State University, Detroit, MI 48201, USA

† Electronic supplementary information (ESI) available. See DOI: https://doi.org/10.1039/d5tc01262g

‡ These authors contributed equally to this work.

N-methyl-2-pyrrolidone (NMP) and dimethylformamide (DMF), which are toxic and have high boiling points of 204 and 153 °C, respectively.[27] It has been confirmed that other solvents are not able to provide sufficient driving force for successful exfoliation due to the large mismatch in total surface tension or polar-to-dispersive (P/D) ratio with $Ta_2Pt_3Se_8$. For this reason, despite its promising properties, the application of $Ta_2Pt_3Se_8$ using solution processing may be limited.

In this study, we introduce a co-solvent exfoliation strategy utilizing an IPA/water mixture to optimize the LPE of $Ta_2Pt_3Se_8$. By employing various volume ratios of each solvent, we finely adjusted the total surface tension, P/D ratio, and dielectric constant of the co-solvent. The exfoliation efficiency using a co-solvent was compared not only with exfoliation in NMP as a single solvent but also with aqueous dispersion using a dispersant. Finally, FET devices were fabricated using $Ta_2Pt_3Se_8$ nanowires exfoliated in the co-solvent, achieving a field-effect mobility of up to 6.76 cm^2 V^{-1} s^{-1} and I_{on}/I_{off} greater than 10^3.

It is believed that these findings will be highly beneficial for identifying optimal solvents for the LPE of various vdW materials, not just $Ta_2Pt_3Se_8$.

Results and discussion

Fig. 1a illustrates the crystal structure of $Ta_2Pt_3Se_8$ and the schematic of the LPE process. $Ta_2Pt_3Se_8$ has a quasi-1D vdW structure that can be exfoliated into smaller units, and detailed information about the crystal structure has been discussed in previous studies. Fig. 1b shows the total surface tension, dielectric constant, and boiling point of the representative exfoliation solvents, namely IPA, water, DMF and NMP. DMF and NMP are known for effectively dispersing graphene, CNTs, TMDCs and $M_2N_3X_8$ due to the well-matched surface tension and dielectric constant.[16,28–32] However, their relatively high boiling points and toxicity limit their use in solution processing
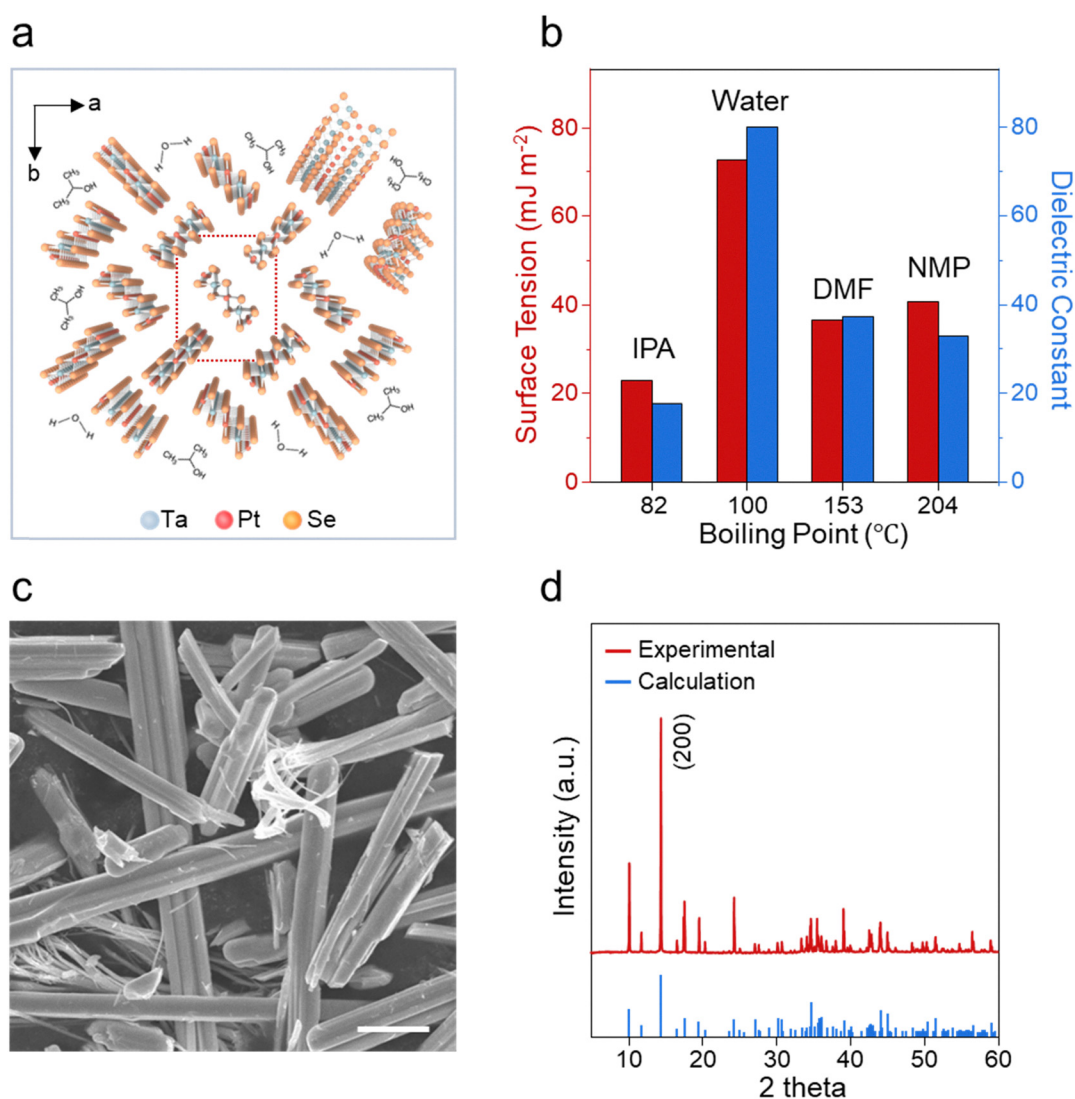

Fig. 1 (a) Crystal structure of the bulk $Ta_2Pt_3Se_8$ crystal and schematic of the LPE process. (b) Information of total surface tension, dielectric constant, and boiling point of IPA, water, DMF and NMP. (c) SEM image of bulk $Ta_2Pt_3Se_8$ crystals (scale bar: 3 μm). (d) XRD result of synthesized bulk $Ta_2Pt_3Se_8$.

and certain applications. On the other hand, although water is non-toxic, it is challenging to achieve good dispersibility using water alone as a solvent. This is because its very high surface tension and dielectric constant cause a large mismatch with the target materials. Therefore, a co-solvent strategy using IPA, which is miscible with water and less toxic, has been widely studied for decades. Bulk $Ta_2Pt_3Se_8$ crystals for LPE were synthesized by a solid-state reaction as previously reported.[24] Fig. 1c and d show the scanning electron microscopy (SEM) image and X-ray diffraction of the obtained bulk $Ta_2Pt_3Se_8$ crystals.

From a thermodynamic perspective, the efficiency of LPE is governed by the intermolecular interactions between the solid and liquid phases. Matching the dielectric constant and minimizing the interfacial surface tension facilitate better immersion and insertion of solvent molecules into the vdW gaps of the layered materials, thereby enhancing exfoliation performance.[33,34] Additionally, according to the OWRK theory, a smaller difference in the P/D ratio between the solvent and solute leads to lower interfacial surface energy. Thereby, the P/D ratio can serve as a useful indicator for evaluating dispersion behavior.[24,35] In this study, we use dielectric constant, surface tension, and P/D ratio as key parameters to explain and assess the dispersion behavior. LPE of $Ta_2Pt_3Se_8$ was performed using 11 different exfoliation solvents with varying IPA content as shown in Table 1. A $Ta_2Pt_3Se_8$ solution with an initial concentration of 1 mg mL^{-1} was ultrasonicated in each solvent and then centrifuged at 6000 rpm for 10 min to obtain the supernatant. Fig. 2a shows photographs of the final $Ta_2Pt_3Se_8$ dispersions with different IPA contents. As seen in the images, the dispersions exhibit particularly dark colors in the IPA content range of 60 to 90%. To precisely compare the concentration of exfoliated $Ta_2Pt_3Se_8$ nanowires in each solvent, UV-visible absorbance was measured as shown in Fig. S1(ESI†). According to the Beer–Lambert law, the absorbance at a specific wavelength is proportional to the concentration of the solute. Therefore, the concentrations of the dispersions were compared based on the absorbance measured at 400 nm. To ensure the consistency of the experiment, each condition was tested three times as summarized in Fig. S2(ESI†). Fig. 2b shows the

changes in absorbance with varying IPA content. The $Ta_2Pt_3Se_8$ dispersions in the range of 60 to 90% exhibited higher absorbance, which is consistent with the results of the final color of the dispersions. To investigate the dispersion behavior of $Ta_2Pt_3Se_8$, the absorbance results were fitted against the total solvent. As shown in Fig. 2c, $Ta_2Pt_3Se_8$ exhibited high exfoliation efficiency in the surface tension range of 22.77 to 24.43 mJ m^{-2}. When examined in terms of the P/D ratio, this corresponds to the range of 0.442 to 0.475 as shown in Fig. 2d. Previous results indicated that the P/D ratio of $Ta_2Pt_3Se_8$ is 0.413, which is approximately close to the P/D ratio of the solvents identified.[27] Finally, as shown in Fig. 2e, the most effective results were obtained with a dielectric constant between 24.12 and 42.78, which is consistent with the high efficiency previously observed in a single-solvent system such as NMP (33.0) and DMF (37.5).[27] These findings demonstrate that the optimal exfoliation solvent can be effectively designed by fine-tuning the properties of the co-solvent rather than relying solely on water and IPA.

To effectively interpret the results of LPE, it is important to analyze not only the concentration, but also the morphology of the exfoliated material. To examine the morphology of the exfoliated $Ta_2Pt_3Se_8$ nanowires, each dispersion was vacuum filtrated onto an anodic aluminum oxide (AAO) membrane and analyzed by SEM. Fig. 3a shows SEM images of the $Ta_2Pt_3Se_8$ nanowires in representative solvent compositions. The width of nanowires in each solvent was compiled into a histogram as shown in Fig. 3b. Overall, after LPE, it was confirmed that the bulk $Ta_2Pt_3Se_8$ crystals were downsized to a scale of several tens of nanometers. However, in the case of the least efficient solvent, 0% IPA, the average width was 67.3 nm with a large deviation. It was observed that the higher the efficiency of the solvent composition in terms of concentration, the smaller the average width of the $Ta_2Pt_3Se_8$ nanowires. Notably, 80% IPA, which exhibited the highest concentration, had the smallest average width of 21.7 nm and the smallest deviation. Fig. 3c shows the width distribution of the produced $Ta_2Pt_3Se_8$ nanowires for all solvent compositions. This indicates that solvents with higher dispersion concentrations tend to produce thinner nanowires with increased uniformity. To confirm the thickness of the $Ta_2Pt_3Se_8$ nanowires exfoliated in the optimal solvent, AFM measurements were conducted. The results showed an average thickness of 11.7 nm as shown in Fig. 3d and Fig. S4(ESI†). All subsequent experiments were carried out using 80% IPA.

To evaluate the effectiveness of our co-solvent approach, we compared it with LPE using NMP and water with an amphiphilic dispersant. Sodium dodecylbenzene sulfonate (SDBS), an anionic dispersant, is commonly used for dispersing CNTs or TMDCs in water.[36,37] Its strong negative charge of sulfonate group creates electrostatic repulsion with surrounding water, allowing aqueous dispersion. Fig. 4a shows photographs of the final dispersions for the three different solvents after LPE under the identical conditions. As shown in Fig. 4b, when comparing concentrations, the IPA–water exhibited an absorbance approximately 1.4 and 6 times higher than NMP and

Table 1 Total surface tension, dispersive component, polar component, polar to dispersive (P/D) ratio and dielectric constant of IPA–water co-solvent with different volume ratios

IPA%	Surface tension (mJ m^{-2})	Dispersive component (mJ m^{-2})	Polar component (mJ m^{-2})	P/D ratio	Dielectric constant
0	72.75	22.10	50.65	2.292	80.1
10	43.90	21.11	22.79	1.080	73.88
20	33.87	19.70	14.17	0.719	67.66
30	28.08	16.94	11.14	0.658	61.44
40	26.16	17.11	9.05	0.529	55.22
50	25.13	16.96	8.17	0.482	49.00
60	24.43	16.56	7.89	0.475	42.78
70	23.78	16.14	7.64	0.473	36.56
80	23.39	16.13	7.26	0.450	30.34
90	22.77	15.79	6.98	0.442	24.12
100	23.00	19.50	3.50	0.179	17.90

17782 | *J. Mater. Chem. C*, 2025, **13**, 17780–17787

This journal is © The Royal Society of Chemistry 2025
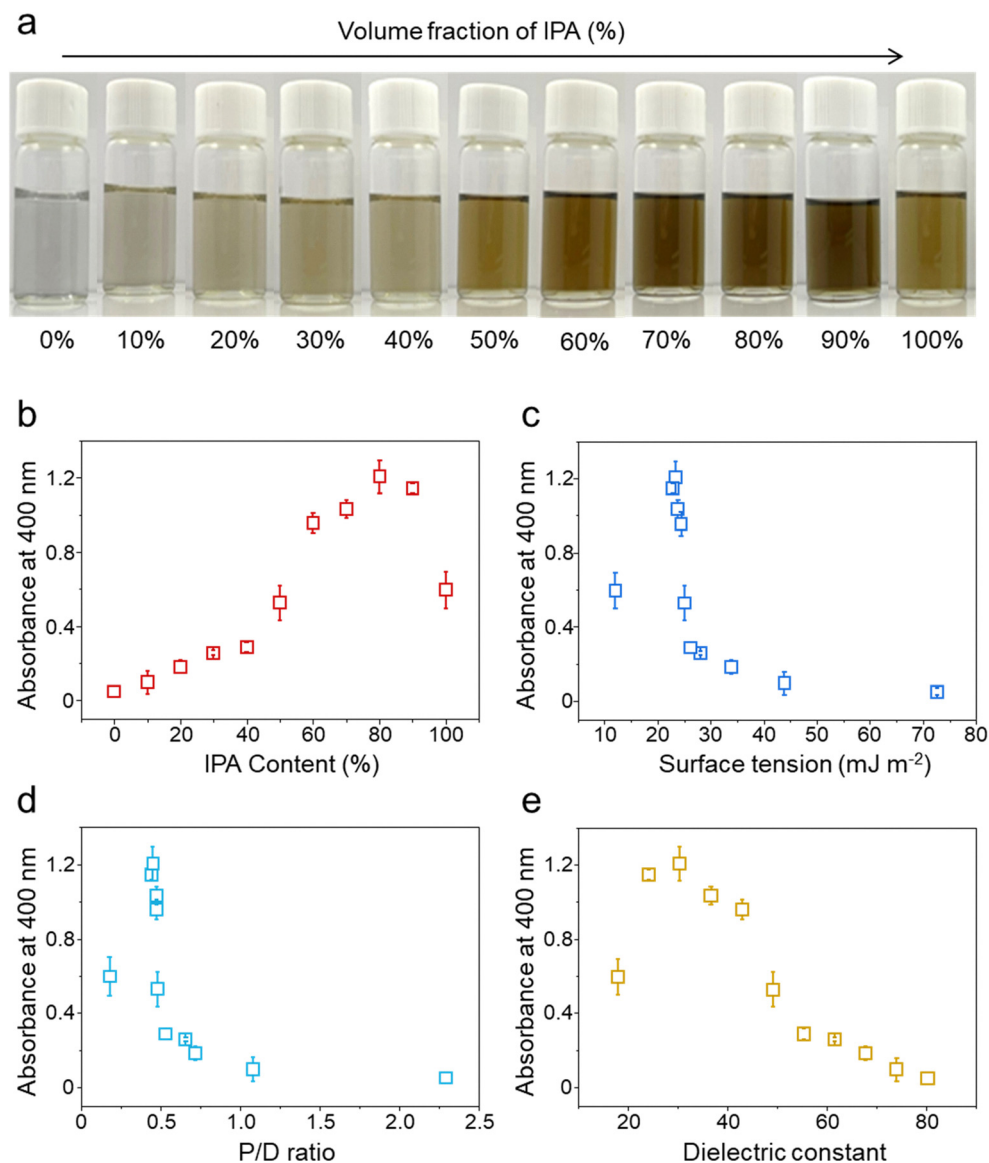
Fig. 2 Dispersion behavior of $Ta_2Pt_3Se_8$ nanowires in different solvent mixtures. (a) Digital images of $Ta_2Pt_3Se_8$ dispersions centrifuged at 6000 rpm after ultrasonication. UV-visible absorbances of $Ta_2Pt_3Se_8$ dispersions at 400 nm as a function of (b) IPA content, (c) surface tension, (d) P/D ratio and (e) dielectric constant.

SDBS–water, respectively. To quantitatively evaluate the exfoliation yield, the extinction coefficient of $Ta_2Pt_3Se_8$ nanowires in IPA/water 80% was determined by fitting absorbance values measured at various concentrations (Fig. S5, ESI†). As a result, the extinction coefficient at 400 nm was determined to be 1841.8 L g^{-1} m^{-1}, and the concentration calculated based on the Beer–Lambert law was 68.1 μg mL^{-1}. This value is approximately 1.39 times higher than the concentration obtained using NMP.

Subsequently, the size of the exfoliated $Ta_2Pt_3Se_8$ nanowires in NMP (23.4 ± 7.0 nm) and SDBS–water (21.3 ± 4.8 nm) was compared to that in IPA–water (21.7 ± 4.9 nm), with no significant difference observed, as shown in Fig. 4c and Fig. S6(ESI†). This demonstrates that the co-solvent approach can achieve significantly higher exfoliation yields in solvents

with lower boiling points and less toxicity. Additionally, X-ray photoelectron spectroscopy (XPS) was performed on $Ta_2Pt_3Se_8$ nanowires exfoliated in the optimum solvent to assess its chemical stability (Fig. S7, ESI†). Each XPS core-level spectrum exhibits a single, well-defined peak without noticeable sub-peaks corresponding to different binding energies. This indicates the absence of oxidation states and confirms that the $Ta_2Pt_3Se_8$ nanowires maintain their chemical stability after the liquid phase exfoliation process.

Finally, to evaluate the electronic properties of the $Ta_2Pt_3Se_8$ nanowires using a co-solvent method, we fabricated FET devices. $Ta_2Pt_3Se_8$/IPA 80% dispersion was spin-coated onto a 100 nm SiO_2/Si substrate, and then Cr/Au (5/50 nm) electrodes were fabricated using standard photolithography and e-beam evaporation. Fig. 5a illustrates the FET device structure and
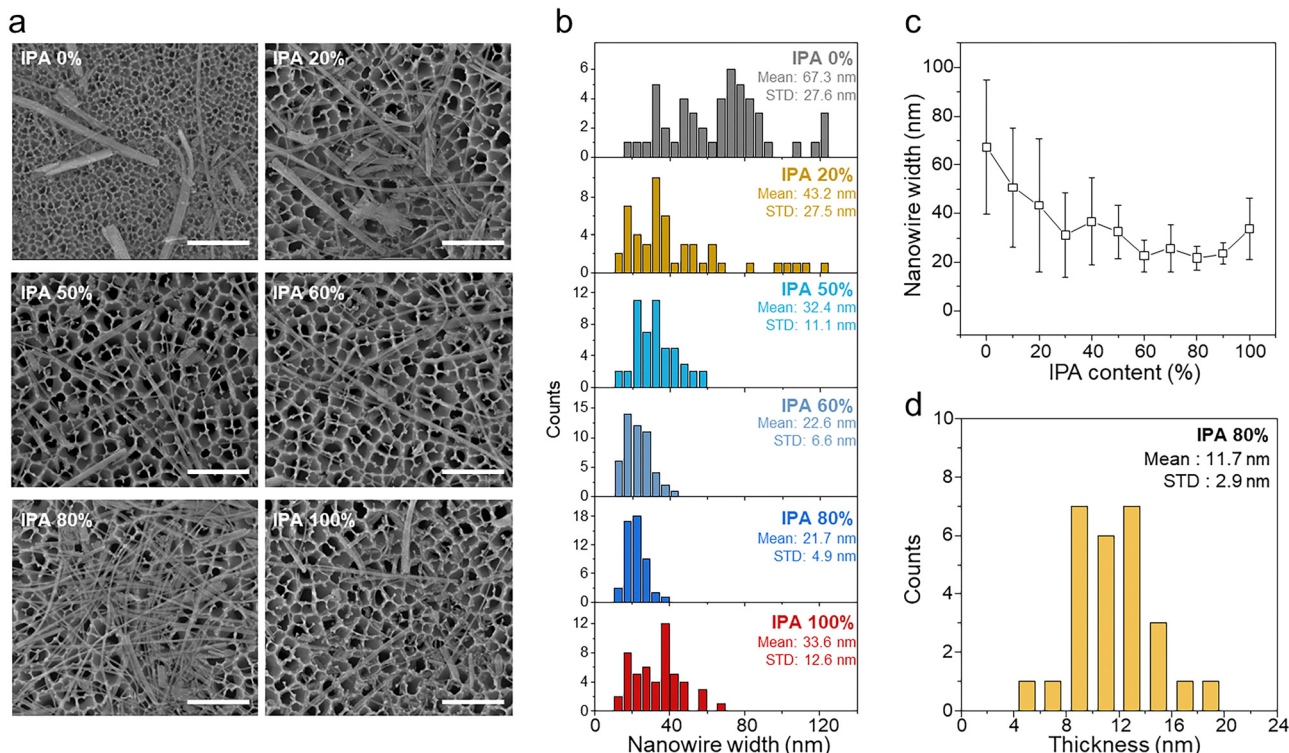
Fig. 3 (a) Representative SEM images of $Ta_2Pt_3Se_8$ nanowires exfoliated in IPA/water co-solvents with different volume ratios (scale bar: 500 nm). (b) Width distribution of $Ta_2Pt_3Se_8$ nanowires as observed from SEM images. (c) Variation in nanowire width as a function of IPA content. (d) Thickness histogram of $Ta_2Pt_3Se_8$ nanowires in 80% IPA as obtained from AFM measurement.
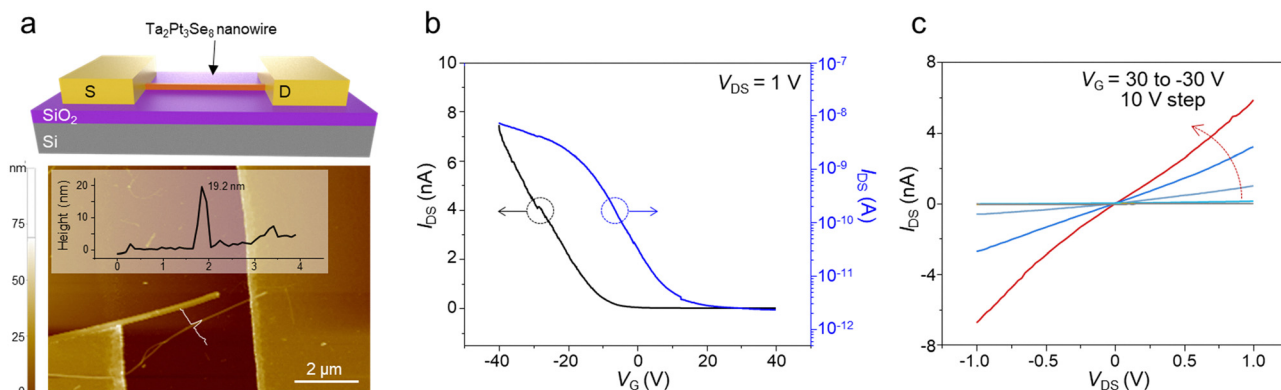

Fig. 4 Comparison of exfoliation efficiency in different types of solvents. (a) Photographs of $Ta_2Pt_3Se_8$ dispersions processed in IPA–water (80% IPA), NMP and SDBS–water. (b) UV-visible absorbance spectra of the dispersions. (c) Average width of $Ta_2Pt_3Se_8$ nanowires exfoliated in NMP and SDBS–water.

shows the corresponding AFM image. Fig. 5b presents the transfer curve (I_{DS}–V_G) measured at room temperature and V_{DS} of 1 V for a 19.2 nm-thick $Ta_2Pt_3Se_8$ nanowire. As in previous reports, it clearly displayed typical p-type transport behavior with I_{on}/I_{off} around 10^3. Its field-effect mobility (μ_{FE}) was extracted using the following equation:

$$\mu_{FE} = (L/WC_{ox}V_{DS})(dI_{DS}/dV_G)$$

Here, L is the channel length, W is the channel width, and C_{ox} is the capacitance of the 100 nm SiO_2 dielectric layer per unit area. The μ_{FE} of the device was 6.76 cm^2 V^{-1} s^{-1}, which is comparable to the mechanically exfoliated $Ta_2Pt_3Se_8$ nanowire.[21] Additionally, the output curves (I_{DS}–V_{DS}) of the device in Fig. 5c show its p-type behavior at varying V_G in the range of 30 to −30 V with an interval of 10 V. The long-term stability of the device was evaluated over a period of 15 days under ambient conditions. As shown in Fig. S8(ESI†), it was confirmed that there was minimal change in the transfer curves, indicating the robustness of the device. Then, to demonstrate the reproducibility of the electrical characteristics,
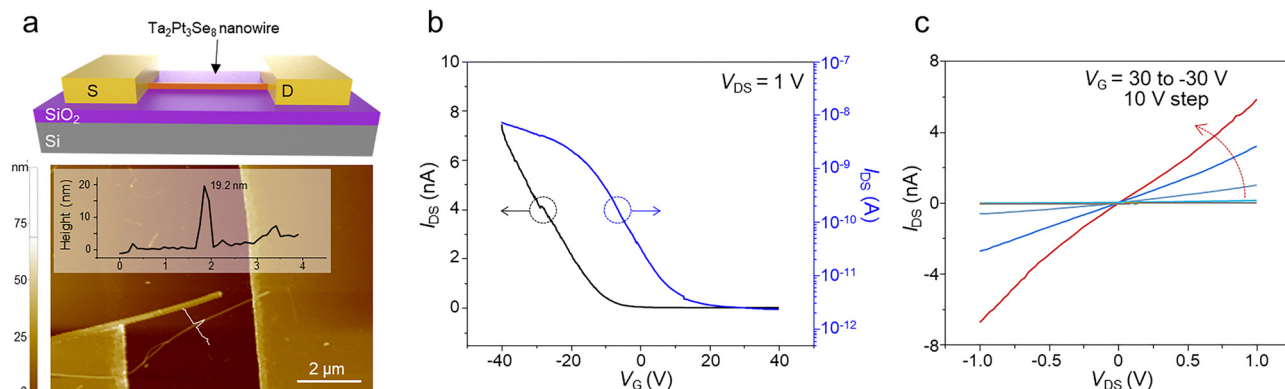
17784 | *J. Mater. Chem. C*, 2025, **13**, 17780–17787

This journal is © The Royal Society of Chemistry 2025

Fig. 5 Device performance of $Ta_2Pt_3Se_8$ nanowires exfoliated in 80% IPA co-solvent. (a) Schematic illustration of $Ta_2Pt_3Se_8$ FET (top) and AFM image of the fabricated device (bottom). (b) Transfer curves of the $Ta_2Pt_3Se_8$ FET in a linear scale (black) and a logarithmic scale (blue) measured at room temperature. (c) Output curves of the $Ta_2Pt_3Se_8$ FET measured in the range of 30 to −30 gate voltage.

the transfer curves were measured across multiple devices. All devices exhibited a distinct p-type response, with I_{DS} decreasing with increasing V_G (Fig. S9, ESI†).

To compare the FET performance based on the exfoliation solvent, devices were fabricated using NMP and SDBS–water solvents. The results from nanowires of similar thickness showed μ_{FE} comparable to those obtained with the co-solvent method as shown in Fig. S10(ESI†). In order to compare device performance not only in single nanowires but also in thin-film structures, we fabricated $Ta_2Pt_3Se_8$ nanowire thin-films by vacuum filtration of IPA–water and SDBS–water dispersions onto AAO membranes. As shown in Fig. S11(ESI†), the 9 × 3 device arrays were deposited on $Ta_2Pt_3Se_8$ thin-films of same thickness using a shadow mask. Then, I–V characteristics were evaluated for all devices of IPA–water and SDBS–water. As shown in Fig. S12(ESI†), IPA–water exhibited a current level nearly one order of magnitude higher than that of SDBS–water, with smaller variation between devices. This can be attributed to the absence of external insulating dispersants that may hinder conductivity.

Conclusions

In this work, we successfully demonstrated a co-solvent exfoliation strategy using an IPA/water mixture as an optimal solvent for LPE of $Ta_2Pt_3Se_8$. The optimal composition of solvents achieved significantly higher exfoliation efficiency compared to traditional single solvent exfoliation in NMP. FETs fabricated with the exfoliated nanowires showed excellent electronic performance, which is comparable to the mechanically exfoliated one. It is believed that this approach can be extended to other vdW materials, paving the way for scalable solution-based processing in various applications.

Materials and method

Synthesis of bulk $Ta_2Pt_3Se_8$ crystals

The bulk $Ta_2Pt_3Se_8$ was synthesized *via* a solid-state reaction using a stoichiometric mixture of Ta powder (99.98%, Alfa

Aesar), Pt powder (99.98% Alfa Aesar) and Se powder (99+%, Alfa Aesar). The mixture was sealed in an evacuated quartz ampoule, heated at temperatures from 1000 °C for 120 h, and cooled to room temperature in furnaces. After the reaction, dark $Ta_2Pt_3Se_8$ powder was obtained.

Characterization

X-ray diffraction (XRD, D8 Advance, Bruker) was performed using Cu-K$_\alpha$ radiation (λ = 0.154 nm) at a scan rate of 5° min^{-1}. Morphological and compositional analyses were conducted using field-emission scanning electron microscopy (FE-SEM, Hitachi, S-4300SE). Topographic analysis was performed in tapping mode using a Park system with Si cantilevers ($\sim$300 kHz resonant frequency) coated with Al (Tap300 Al, Budget Sensors Inc.) with a scan rate of $\sim$0.4 Hz. UV-visible absorbance was measured using a UV-vis-spectrophotometer (Agilent Technologies Inc., Agilent 89090A).

Liquid phase exfoliation

The LPE of $Ta_2Pt_3Se_8$ was carried out through ultrasonication and centrifugation. The bulk crystal and the selected solvent were added to a 40 mL vial at an initial concentration of 1 mg mL^{-1}. Then, ultrasonication was performed in an ice bath using a probe sonicator (VC505, Sonics and Materials Inc.) for 10 min at intervals of 2 s on/2 s off, this was followed by bath sonication (B2005S-68K, 68 kHz, 200 W, KODO Technical) for 3 h. The resulting dispersions were centrifuged at 6000 rpm for 10 min to remove larger crystals that were not fully exfoliated. After centrifugation, the supernatant solution was used for further characterization.

Device fabrication

$Ta_2Pt_3Se_8$ nanowires exfoliated in 80% IPA were chosen for device fabrication. The nanowires were collected from 3000 rpm centrifugation to ensure the length of nanowires. $Ta_2Pt_3Se_8$ dispersion was spin-coated on a highly doped SiO_2 (100 nm)/Si substrate. The device was patterned using the standard photolithography method, and the Cr/Au (5/50 nm) electrodes were

This journal is © The Royal Society of Chemistry 2025

J. Mater. Chem. C, 2025, **13**, 17780–17787 | **17785**

deposited using an e-beam evaporator under high vacuum conditions.

Author contributions

K. H. C. and D. K. contributed equally to this work. J. K., C. W. and X. Z. supported the synthesis and analysis. Y. H. K., Y. K. and H.-S. B. supported the exfoliation and analysis. K. I. K., J. S. P. and S. J. supported the device fabrication. J. C., H.-S. O. and J.-H. L. supported data curation. H. K. Y. and J.-Y. C. supervised the whole project.

Conflicts of interest

There are no conflicts to declare.

Data availability

The authors confirm that the data supporting the findings of this study are available within the article and ESI.†

Acknowledgements

References

1 X. Cai, Y. Luo, B. Liu and H.-M. Cheng, *Chem. Soc. Rev.*, 2018, **47**, 6224–6266.

2 V. Nicolosi, M. Chhowalla, M. G. Kanatzidis, M. S. Strano and J. N. Coleman, *Science*, 2013, **340**, 1226419.

3 K. R. Paton, E. Varrla, C. Backes, R. J. Smith, U. Khan, A. O'Neill, C. Boland, M. Lotya, O. M. Istrate and P. King, *Nat. Mater.*, 2014, **13**, 624–630.

4 R. Sharma, A. Kumar, A. Dawar, S. Ojha, A. Mishra, A. Goyal, R. Laishram, V. G. Sathe, R. Srivastava and O. M. Sinha, *Trans. Electr. Electron. Mater.*, 2023, **24**, 140–148.

5 C. Tan, X. Cao, X.-J. Wu, Q. He, J. Yang, X. Zhang, J. Chen, W. Zhao, S. Han and G.-H. Nam, *Chem. Rev.*, 2017, **117**, 6225–6331.

6 R. Sardar, A. M. Funston, P. Mulvaney and R. W. Murray, *Langmuir*, 2009, **25**, 13840–13851.

7 D. Zhou, M. Lin, Z. Chen, H. Sun, H. Zhang, H. Sun and B. Yang, *Chem. Mater.*, 2011, **23**, 4857–4862.

8 S. Baruah and J. Dutta, *Sci. Technol. Adv. Mater.*, 2009, **10**, 013001.

9 H.-S. Qian, S.-H. Yu, J.-Y. Gong, L.-B. Luo and L.-F. Fei, *Langmuir*, 2006, **22**, 3830–3835.

10 M. Naqi, K. H. Choi, H. Yoo, S. Chae, B. J. Kim, S. Oh, J. Jeon, C. Wang, N. Liu and S. Kim, *NPG Asia Mater.*, 2021, **13**, 46.

11 T. Y. Kim, C. Woo, K. H. Choi, X. Dong, J. Jeon, J. Ahn, X. Zhang, J. Kang, H.-S. Oh and H. K. Yu, *Nanoscale*, 2022, **14**, 17365–17371.

12 K. R. G. Lim, M. Shekhirev, B. C. Wyatt, B. Anasori, Y. Gogotsi and Z. W. Seh, *Nat. Synth.*, 2022, **1**, 601–614.

13 V. Natu, J. L. Hart, M. Sokol, H. Chiang, M. L. Taheri and M. W. Barsoum, *Angew. Chem.*, 2019, **131**, 12785–12790.

14 Y. Sun, F. Alimohammadi, D. Zhang and G. Guo, *Nano Lett.*, 2017, **17**, 1963–1969.

15 M. P. Kumar, S. Raga, S. Chetana, K. Avinash, A. Dey and D. Rangappa, *Trans. Electr. Electron. Mater.*, 2023, **24**, 235–241.

16 D. Rhee, D. Jariwala, J. H. Cho and J. Kang, *Appl. Phys. Rev.*, 2024, **11**, 021310.

17 X. Zhang, Z. Lai, C. Tan and H. Zhang, *Angew. Chem., Int. Ed.*, 2016, **55**, 8816–8838.

18 L. Pan, Y. T. Liu, X. M. Xie and X. Y. Ye, *Small*, 2016, **12**, 6703–6713.

19 R. A. Shaukat, A. M. Tamim, G. T. Hwang and C. K. Jeong, *Trans. Electr. Electron. Mater.*, 2024, **25**, 123–140.

20 J. Teeter, N. Y. Kim, T. Debnath, N. Sesing, T. Geremew, D. Wright, M. Chi, A. Z. Stieg, J. Miao and R. K. Lake, *Adv. Mater.*, 2024, **36**, 2409898.

21 S. Oh, S. Chae, M. Kwon, J. Ahn, C. Woo, K. H. Choi, J. Jeon, X. Dong, T. Y. Kim and G. Asghar, *ACS Nano*, 2022, **16**, 8022–8029.

22 K. H. Choi, J. Jeon, B. J. Jeong, S. Chae, S. Oh, C. Woo, T. Y. Kim, J. Ahn, J. H. Lee and H. K. Yu, *Adv. Mater. Interfaces*, 2022, **9**, 2200620.

23 X. Liu, J. Liu, L. Y. Antipina, J. Hu, C. Yue, A. M. Sanchez, P. B. Sorokin, Z. Mao and J. Wei, *Nano Lett.*, 2016, **16**, 6188–6195.

24 B. J. Jeong, K. H. Choi, J. Jeon, S. O. Yoon, Y. K. Chung, D. Sung, S. Chae, S. Oh, B. J. Kim and S. H. Lee, *Nanoscale*, 2021, **13**, 17945–17952.

25 T. Wang, Y. Zhu, Z. Mao and Y.-Q. Xu, *ACS Appl. Nano Mater.*, 2021, **4**, 1817–1824.

26 K. S. Novoselov, A. K. Geim, S. V. Morozov, D.-E. Jiang, Y. Zhang, S. V. Dubonos, I. V. Grigorieva and A. A. Firsov, *Science*, 2004, **306**, 666–669.

27 K. H. Choi, S. H. Lee, J. Kang, X. Zhang, J. Jeon, H.-S. Bang, Y. Kim, D. Kim, K. I. Kim and Y. H. Kim, *ACS Appl. Mater. Interfaces*, 2024, **16**, 35463–35473.

28 J. N. Coleman, *Acc. Chem. Res.*, 2013, **46**, 14–22.

29 A. Ciesielski and P. Samorì, *Chem. Soc. Rev.*, 2014, **43**, 381–398.

30 C. Pramanik, J. R. Gissinger, S. Kumar and H. Heinz, *ACS Nano*, 2017, **11**, 12805–12816.

31 M. K. Fathy, A. H. Zaki, H. A. Shawkey and H. R. Tantawy, *Trans. Electr. Electron. Mater.*, 2024, **25**, 732–744.

32 S. Polat, M. Mashrah and A. Maksur, *Trans. Electr. Electron. Mater.*, 2024, **25**, 801–810.

33 J. Shen, J. Wu, M. Wang, P. Dong, J. Xu, X. Li, X. Zhang, J. Yuan, X. Wang, M. Ye, R. Vajtai, J. Lou and P. M. Ajayan, *Small*, 2016, **12**, 2741–2749.

17786 | *J. Mater. Chem. C*, 2025, **13**, 17780–17787

This journal is © The Royal Society of Chemistry 2025

34 J. Shen, Y. He, J. Wu, C. Gao, K. Keyshar, X. Zhang, Y. Yang, M. Ye, R. Vajtai, J. Lou and P. M. Ajayan, *Nano Lett.*, 2015, **15**, 5449–5454.

35 M. Wang, X. Xu, Y. Ge, P. Dong, R. Baines, P. M. Ajayan, M. Ye and J. Shen, *ACS Appl. Mater. Interfaces*, 2017, **9**, 9168–9175.

36 V. C. Moore, M. S. Strano, E. H. Haroz, R. H. Hauge, R. E. Smalley, J. Schmidt and Y. Talmon, *Nano Lett.*, 2003, **3**, 1379–1382.

37 S. Chae, S. Oh, K. H. Choi, J. Jeon, Z. Liu, C. Wang, C. Lim, X. Dong, C. Woo and G. Asghar, *ACS Appl. Bio Mater.*, 2020, **3**, 3992–3998.

This journal is © The Royal Society of Chemistry 2025

J. Mater. Chem. C, 2025, **13**, 17780–17787 | **17787**